Molecular dynamics simulations of the evaporation of particle-laden droplets

Weikang Chen, Joel Koplik, and Ilona Kretzschmar

Molecular dynamics simulations of the evaporation of particle-laden droplets

Weikang Chen[1,3],[*] Joel Koplik[1,3],[†] and Ilona Kretzschmar[2][‡]

Benjamin Levich Institute[1] and Departments of Chemical Engineering[2] and Physics[3]

City College of the City University of New York, New York, NY 10031

We use molecular dynamics simulations to study the evaporation of particle-laden droplets on a heated surface. The droplets are composed of a Lennard-Jones fluid containing rigid particles, which are spherical sections of an atomic lattice, and heating is controlled through the temperature of an atomistic substrate. We observe that sufficiently large (but still nano-sized) particle-laden drops exhibit contact line pinning, measure the outward fluid flow field which advects particles to the drop rim, and find that the structure of the resulting aggregate varies with inter-particle and droplet-wall interactions. The profile of the evaporative fluid flux is measured with and without particles present, and is also found to be in qualitative but not quantitative agreement with earlier theory. The compatibility of the deposit patterns in simple nanoscale calculations and micron-scale experiments indicates that molecular simulation may be used to predict aggregate structure in evaporative growth processes.

[*] wchen@ccny.cuny.edu

[†] koplik@sci.ccny.cuny.edu

[‡] kretzschmar@ccny.cuny.edu

I. INTRODUCTION

The evaporation of a sessile droplet on a hot surface is a key problem in fluid mechanics, relevant both to theoretical issues in heat transfer and to practical questions in materials processing. The evaporation of a *particle-laden* droplet raises the additional issue of the structure of the resulting solid aggregate, and, going further, offers the possibility of controlling this structure by means of anisotropic (*e.g.*, Janus) surface properties [1]. A familiar and paradigmatic example of this process occurs in coffee stains, where the residue of evaporated droplets takes the form of a ring-like deposit of grains at the rim. Experiments by Deegan and collaborators [2] focused attention on this "coffee ring problem" several years ago, and subsequent work [3–6] established the ubiquity of the process, while numerous theoretical studies have addressed the dynamics [7–10, 13, 14]. A complete understanding of the problem is not yet available however: experiments cannot measure everything in a small, time-dependent, multiphase droplet, while most theoretical treatments require approximations to deal with an evaporating particle-laden drop.

The difficulty of understanding the droplet evaporation mostly comes from the complex interaction between the three phases: the solid wall, the liquid droplet itself and its vapor. The interaction of solid and liquid gives rise to a thermal effect: heat transfer from the wall to the droplet. The interactions within the liquid cause a hydrodynamic effect: particle convection due to the internal flow. Interactions between liquid and vapor, and in particular the temperature contrast, produces an evaporative flux from the droplet surface. In addition, temperature variation along the liquid-vapor interface may yield a Marangoni flow due to surface tension variation. The interplay of these effects control the structure of the particle deposit.

In this paper we use molecular dynamics (MD) simulations to simulate the evaporation of droplets containing colloidal particles, having either uniform or Janus-like surface properties. One goal is to test whether the phenomena found in micron-sized particle systems persist down to nanometer scales; in this way we hope to extend the size range in which controlled aggregate structures may be produced by droplet evaporation. A second goal is to test the validity of some of the underpinnings of the theoretical analyses used in the problem. Since MD simulations provide detailed atomic-scale information: concentration, temperature and fluid flow fields are available even during the rapid heterogeneous processes occurring in

evaporation. Furthermore, key parameters such as the strength of the interaction between wall and liquid, liquid and liquid, and liquid and particles are easily varied here, serving as a convenient virtual laboratory for addressing the questions raised above. The difficulties of applying uncertain constitutive relations are absent, although replaced to some degree by the problem of extracting a robust signal from a relatively small sample in a fluctuating environment. More generally, our goal is to establish the ability of these relatively basic simulations of moderate scale systems to predict phenomena occurring in droplet evaporation and guide experimental investigations. As usual in MD simulations, the length and time scales of the simulations are much shorter than those of laboratory experiments, but the phenomena of deposition and pattern formation studied here are quite similar.

II.   MOLECULAR DYNAMICS SIMULATION

A.   Modeling assumptions

The simulations use standard molecular dynamics (MD) techniques [16–18] and generic interactions of Lennard-Jones form,

$$V(r_{ij}) = 4\epsilon \left[\left(\frac{\sigma}{r_{ij}} \right)^{12} - c_{ij} \left(\frac{\sigma}{r_{ij}} \right)^{6} \right] \tag{1}$$

The parameter c_{ij} can be used to adjust the strength of the interaction between atomic species i and j, but for simplicity in most simulations we set it to unity and we assume that all fluid-fluid and fluid-particle interactions have the same interaction potential, along with the same mass m and approximate atomic diameter σ. The calculations are nondimensionalized using ϵ, σ and m as energy, length and mass scales, respectively, and the resulting time scale is $\tau = \sigma(m/\epsilon)^{1/2}$. Typical numerical values are $\sigma \sim 0.3$nm, $\tau \sim 2$ps and $\epsilon \sim 120k_B$, where k_B is Boltzmann's constant, and temperatures are measured in units of ϵ/k_B. The fluid atoms in the liquid or vapor obey ordinary Newtonian dynamics with the force arising from the interaction with other atoms (within a cutoff radius of 2.5 σ). Newton's equations are integrated using a predictor-corrector method with a time step of 0.005τ. The suspended particles are spherical sections of an atomic cubic lattice containing all atoms within a certain radius of a center; here the atomic density is 0.8, the radius is 2 and the particles contain 32 atoms. Two types of particles are considered in this paper – "plain," with uniform surface

properties, and "Janus", which have different interactions on each hemisphere. To implement Janus particles, we make the atoms in only one hemisphere of a particle attractive to other particle atoms while those in the other hemisphere have only the repulsive r^{-12} interaction; all particle atoms attract the fluid and wall atoms with unit strength. (Specific examples might be a particle with a uniform shell in which one half has a magnetic component, or a gold-coated polystyrene particle where the contact angles on gold and polystyrene are comparable but the charge distribution differs.) The particles move as rigid bodies, where the net force and torque on each particle is computed by summing the interatomic forces between its atoms and the neighboring fluid atoms, and the motion is given by Newton's and Euler's equations. Quaternion variables are used to describe the particle orientations [16]. The solid substrate is made of atoms coupled to lattice sites by a linear spring of stiffness $100\epsilon/\sigma^2$.

Initially the drop consists of a hemispherical cap of 72,236 fluid atoms placed above a solid wall consisting of a single layer of fcc unit cells. The drop contains 119 particles of 32 atoms each, centered at random positions within the cap. The simulation box dimensions are 130x130 in the $x - y$ plane of the wall, and 90 in the vertical z-direction. The entire system is prepared by gradually raising the temperature from 0.5 to 1.0 over a 10τ interval, following which the liquid is maintained at this temperature for an additional 100τ, using a Nosé-Hoover thermostat. During this period the walls of the simulation box are reflecting. The structure of the system at this stage is shown in Fig. 1 in terms of time-averaged density profiles of fluid atoms and particles, and a snapshot is given in Fig. 2a. These densities are computed by counting the number of atoms or particles in a three dimensional array of concentric hemispherical sampling bins centered at the middle of the drop at the wall (subsequent profiles in this paper are given in cylindrical coordinates). The density profile for the fluid atoms shows a liquid hemisphere of density 0.85 surrounded by vapor of density 0.04. These values are roughly consistent with the measured phase diagram for the Lennard-Jones system [19], but some deviation occurs because of the presence of the wall. Note that during the preparation stage the particles remain approximately uniformly distributed in the interior of the drop, as indicated in the figure, although there are too few particles present to produce a smooth curve.

The drop actually tends to spread slightly during preparation, because when the fluid-wall interaction has unit strength ($c_{fw} = 1$ in Eq. 1) the liquid is completely wetting and would
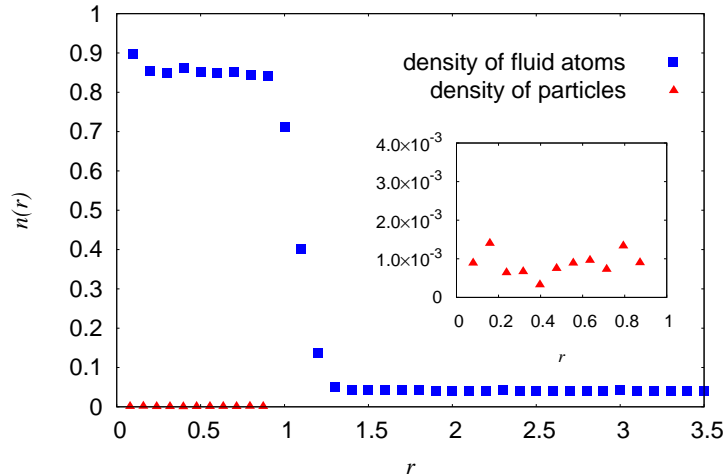
FIG. 1. (Color online) Equilibrated drop structure before evaporation: time-averaged density of fluid (main figure) and particles (inset) as a function of (three-dimensional) distance from the center of the drop at the wall.

eventually spread to cover the substrate [20]. However, this spreading is very slow, with drop contact radius varying as $t^{1/10}$ [21], and is preempted by the more rapid evaporation process. As a check, we have also simulated a partially-wetting liquid, with $c_{fw} = 0.75$ and a 90° contact angle [20], and found no significant change in the evaporation dynamics reported below. Another potential complication is that the atoms in the particles attract each other and the particles would eventually form clusters, but this process is driven by the slow Brownian motion of the particles and also occurs on time scales well beyond those of evaporation.

To evaporate the drop, the temperature of the wall is ramped further to 1.2 over a 10τ interval and maintained at that value by a constant kinetic energy thermostat, while the fluid temperature is allowed to vary. (The simplest thermostat is used for the wall since our focus is the dynamics of the liquid in the unthermostatted drop.) The liquid expands slightly during the temperature ramp and then, as seen in Fig. 2, the drop shrinks monotonically as it emits vapor, and eventually disappears due to evaporation. The structure of the deposit is discussed below; see in particular Fig. 8. The time-dependent vapor density is monitored during the simulation, and evaporating fluid atoms which arrive at the boundary of the simulation box are either bounced back or deleted so as to maintain a constant vapor environment for the drop at the same density, 0.04, as at the end of the preparation stage.
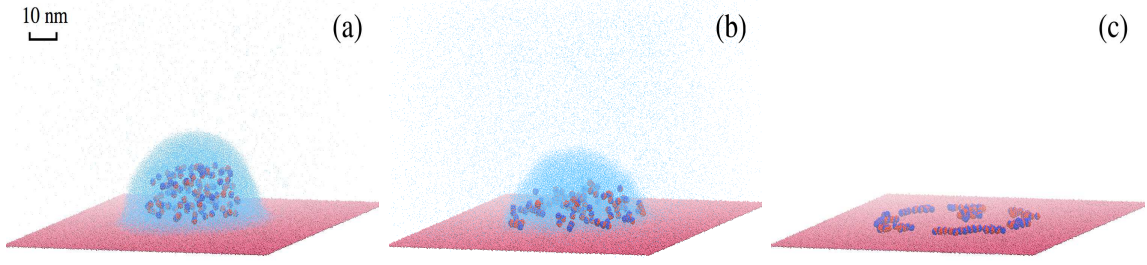
FIG. 2. (Color online) Stages in the evaporation of a Janus particle-laden droplet: (a) after 50τ, (b) 500τ and (c) 1000τ. The fluid atoms in the drop are shown as cyan (light) dots, the solid atoms in the substrate are red (dark) dots, and the Janus particles are filled circles whose two sides are red (medium grey) and blue (dark grey).

B. Analysis of evaporation

Our concern here is the shape evolution and particle flux produced during evaporating of a droplet placed on a heated surface, and in particular the effects of suspended particles. We observe that there is little difference between plain and Janus particles in this regard (only) and in this subsection we refer for simplicity to Janus particles alone.
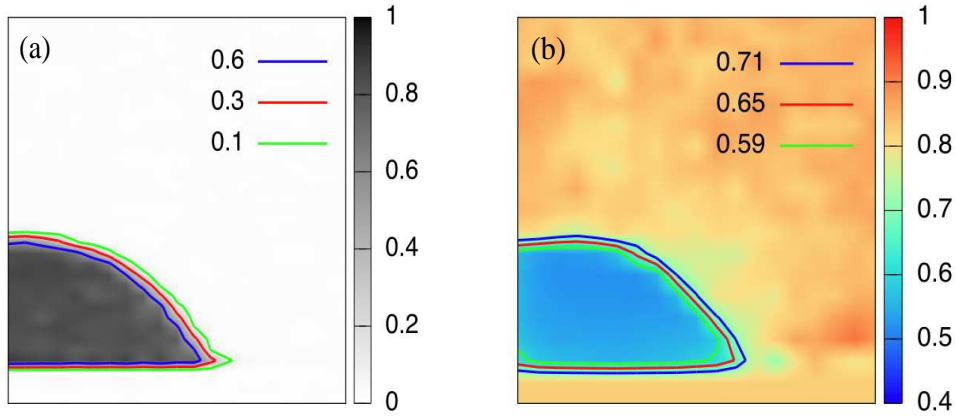

FIG. 3. (Color online) Contour plots of (a) density and (b) temperature in cylindrical coordinates, in a typical simulation with Janus particles at time 300τ. The corresponding plots for plain particles are similar. The contour values of density decrease in going from drop to vapor, while those of temperature increase.

We first consider the temperature and density distributions within the system. The

drop is observed to maintain an approximate spherical cap shape as it evaporates, so in the analysis we use a cylindrical (r, ϕ, z) coordinate system with the vertical z-axis through the center of the drop, and divide the simulation domain into a two-dimensional array of concentric circular rings in the radial r and vertical directions. We record the number of particles and their velocity and temperature in each ring and average over a 10τ time interval. The result for a typical simulation is shown in Fig. 3. We see that both density and temperature are fairly uniform within the drop despite the presence of the particles, with higher fluctuations in the vapor region due to having fewer molecules there to average over. The temperature at the rim is slightly higher than in the interior due to the fact that the escaped vapor atoms need a higher kinetic energy on average. Note however that the temperature variation *along* the liquid-vapor interface is fairly weak, and we therefore neglect Marangoni effects in the subsequent discussion. The density varies smoothly between the bulk liquid and bulk vapor values, with most of the transition occurring near the interfacial region, and the latter maintains a nearly-constant thickness along the drop surface. An important observation is that the liquid-vapor interface is not a perfect spherical cap and deviates notably at the foot of the drop, reflecting the completely-wetting nature of the liquid.
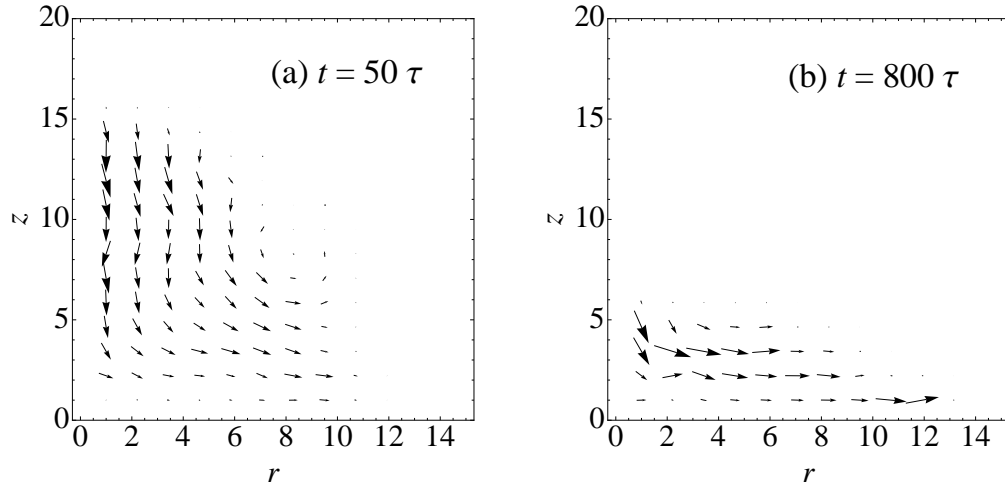

FIG. 4. Velocity field in cylindrical coordinates in an evaporating Janus particle-laden droplet at (a) early and (b) late times; the solid occupies the region $z < 0$.

During evaporation, the particles are advected first towards the substrate and subsequently to the rim of the droplet where they deposit. The contact line itself remains pinned.

The connection between liquid and particle motion is indicated by the velocity field shown in Fig. 4: the fluid moves downward over most of the drop and radially outward near the substrate. The origin of the flow that drives particles to the rim is, it is believed [2], contact line pinning coupled to the fact that the evaporative flux is largest at the edges of the drop. The liquid must supply this flux as the droplet shrinks down, and the geometry of the situation requires a strong outward flow field, as seen in Fig. 4.
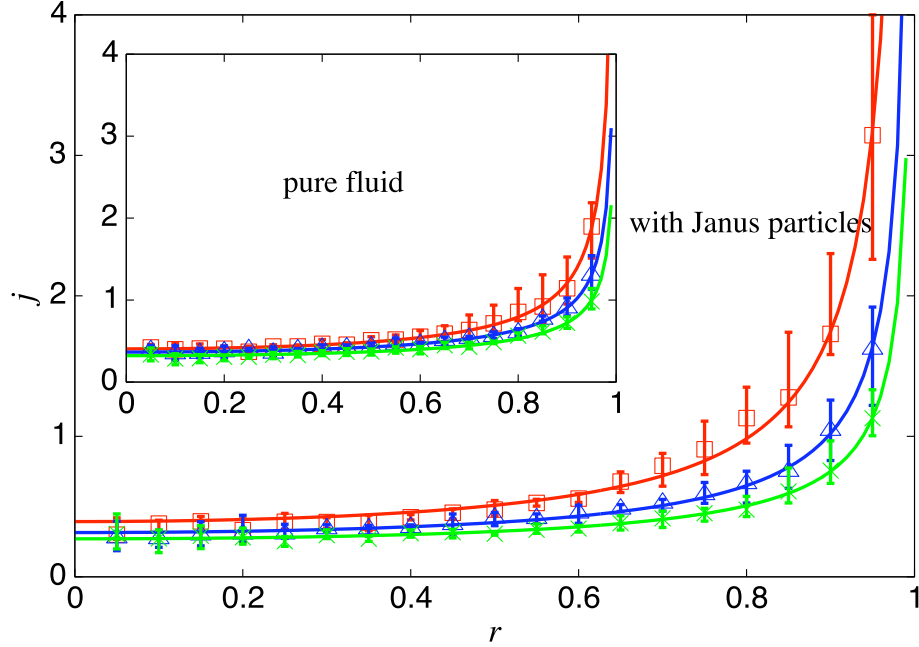

FIG. 5.   (Color online) Evaporative vapor flux vs. scaled radius for Janus particle laden-drops and, in the inset, for pure fluid drops. (The analogous plot for plain particles is similar to the Janus case.) The three curves are fits to Eq. 2 at times 300τ ($\times$, green), 400τ ($\triangle$, blue) and 500τ ($\square$, orange). The error bars indicate the statistical uncertainty in a sample of five realizations.

We have measured the evaporative flux both for pure liquid and particle-laden drops, and obtained Fig. 5, which shows j at the three successive times indicated. Each plot is an average over a short (10τ) interval centered at 300, 400 and 500τ. Averaging is necessary to smooth the fluctuations, and longer averaging periods would be more effective, but the drop shape changes too much over longer intervals. The entire evaporation process lasts for about 1000τ (roughly 2 ns) for the Janus case, and slightly longer for pure fluid evaporation, but the data at later times involves fewer and fewer evaporating atoms and is too noisy for analysis. The results shown above are based on an ensemble average of 5 realization. The

ordinate in Fig. 5 is radial position divided by the current drop (x-y) radius, and varies between 0 and 1. While the radius is constant (except for fluctuations) in the particle-laden case, the radius of the pure fluid drop decreases with time. Note the rapid increase in flux as the contact line is approached ($r \to 1$).

We have attempted to relate the simulation data to a popular "Lens" model from the literature. This approach assumes that the vapor concentration satisfies a steady-state diffusion equation with an evaporative flux proportional to the concentration gradient, and solves the resulting boundary value problem by analogy to the electrostatics of a lens held at fixed potential [11–14]. The outcome is

$$j(r;\theta) = j_0(\theta) \left(1 - \frac{r^2}{R^2} \right)^{-\lambda(\theta)} \qquad \lambda(\theta) = \frac{1}{2} \left(1 - \frac{\theta}{\pi - \theta} \right) \qquad (2)$$

where the flux $j(r;\theta)$ is the number of atoms crossing a sampling ring just outside and parallel to the drop surface, centered at (cylindrical coordinate) radius r, per unit time and per unit area. The flux depends on the drop contact radius R and the contact angle θ, the latter varying as the droplet evaporates. The key point is that for $\theta < \pi/2$ the (mathematical) vapor flux diverges at the edge of the droplet. Of course, there is no real singularity in a physical problem, and one expects j to be cut off at a small (molecular) scale. The Lens model qualitatively accounts for the behavior of the evaporative flux: the functional form in Eq. 2 fits the data in Fig. 5 well. The simulations are also consistent with the other aspects of the theory such as the variation of contact angle and drop volume with time, shown in Fig. 6 for both the pure and particle-laden fluid cases. (The contact angle is obtained by fitting snapshots of the drop to a spherical cap, and the volume is estimated by counting the number of atoms within it, and using the measured density.) However, the formula fails to quantitatively describe the simulations. The exponents $\lambda(\theta)$ obtained in fitting the pure fluid data are 0.48, 0.55 and 0.65 at times 300, 400 and 500τ, respectively, but Eq. 2 does not permit values $\lambda > 1/2$. The flux is slightly more singular for the particle-laden drop: the fitted values of λ are 0.61, 0.71 and 0.83 for the same three times. The stronger divergence is presumably the outcome of the contact line pinning, since the particles at the edge prevent the liquid from receding.

The origin of the discrepancy requires some discussion. One possibility is that the flux is not measured accurately at the edge of the drop, where evaporating atoms travel nearly parallel to the surface, and indeed the error bars in our flux measurements are distinctly
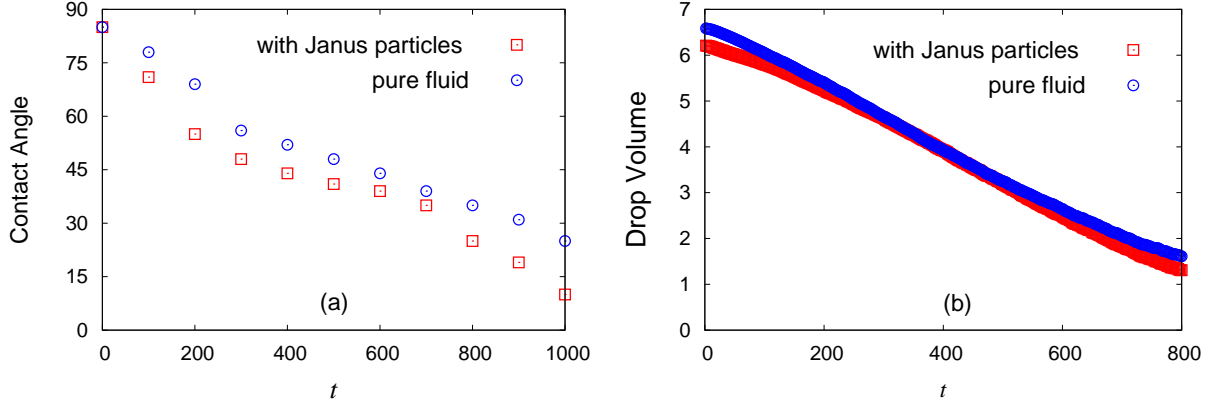
FIG. 6. (Color online) Variation of (a) contact angle and (b) droplet volume with time, for evaporating drops with (lower curves, □) and without (upper curves, ⊙) Janus particles.

larger at the edge. However, the fit is quite good at lower values of radius r, and even if we delete the less-certain points at large r from the fitting procedure, the resulting exponents change only by about 4%. Along the same line, the density contour plot indicates that the drop shape deviates from a circular cap at the three-phase contact line at the foot of the drop, a feature not accounted for in the theoretical prediction. In Fig 7 examples of this region are shown in molecular detail for both pure-liquid and particle-laden drops. The liquid drop shows a fairly smooth circular interface with a transition zone of modest thickness along most of the surface, and a small foot which reflects the fact that the liquid is completely wetting and the drop would spread under isothermal conditions. In the presence of particles, however, the liquid-vapor interface is distinctly less regular everywhere. If the details of the interface shape were responsible for the discrepancy between theory and simulation in the evaporative flux one would expect the results for pure and particle-laden drops to differ significantly, but in fact they do not.

A second possible source of discrepancy is that the simulation conditions may deviate from the assumptions leading to Eq. 2. In particular, the liquid density and interface temperature are assumed to be uniform and the drop shape is assumed to be a spherical cap, whereas the simulation protocol does not explicitly enforce this behavior. Nonetheless, as shown in Fig. 3, we do observe a roughly spherical shape and constant density and temperature throughout most of the evaporating drop. Slight variations occur at the foot of the drop, but as noted above this region does not control the fitted exponents. A more likely explanation
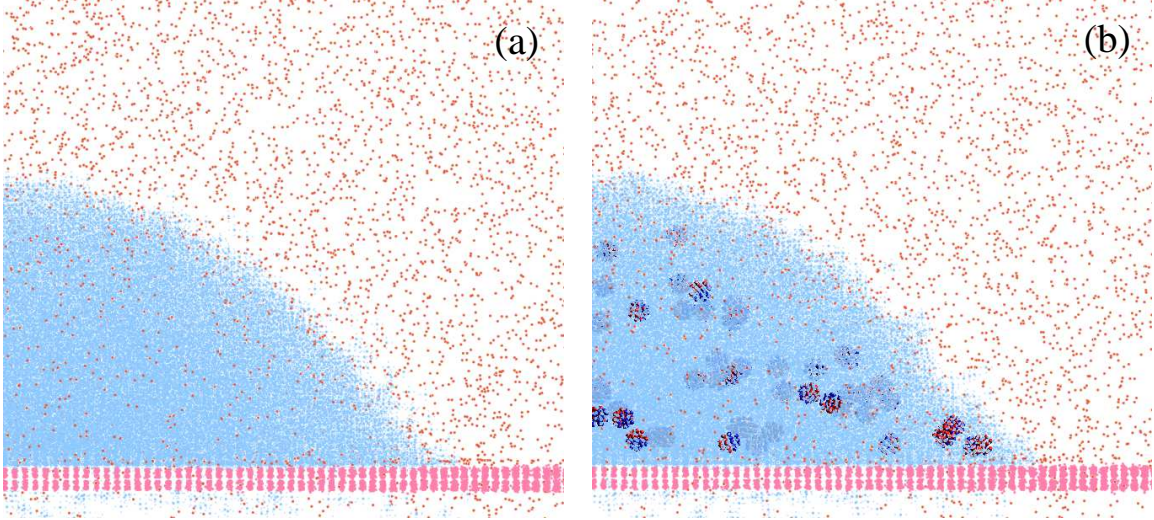
FIG. 7. (Color online) Views of the edge of evaporating droplets at molecular resolution: (a) pure liquid and (b) particle-laden drops.

is that the evaporation process is poorly approximated by the Laplace equation used in the theoretical analysis. In particular, the Péclet number $Pe = vR/D$ in these simulations is appreciable: a peak value can be estimated as $Pe \sim (1.0) \cdot (50)/(0.2) \sim 250$ using the measured largest fluid velocity $v \sim 1.0$, the drop contact radius R, and an earlier calculation of the molecular diffusivity D [23]. In consequence, the advective derivative term $\vec{v} \cdot \nabla c$ in the full concentration equation is required here, which would alter the predicted exponents in Eq. 2. In larger (millimeter-sized) drops, the velocities are likely to be smaller since the relative temperature differences are less, and this complication may be absent.

A common alternative approach to the evaporative flux assumes that vapor diffusion is rapid and instead transport processes within the liquid control evaporation [8, 24]. The resulting nonequilibrium one-sided ("Neos") model is most often used in modeling thin liquid films in the limit of weak surface height variation, which is not entirely appropriate to the geometry of nano-size droplets. Furthermore, the starting point is an assumption that the local evaporative flux is proportional to the difference between the interface temperature and the saturation temperature of the liquid. In our simulations, however, we observe a nearly constant interfacial temperature and the model would predict a constant flux along the interface, which we do not observe. If we nonetheless attempt to fit our flux data to the Neos expression for the flux, $j(r) = j_0/(K + h(r))$, where j_0 and K are constants and $h(r)$

is the local height of the drop, the result is a very poor fit.

C. Deposition pattern

The pattern formed by deposited particles after evaporation *is* sensitive to the interaction between the particles, and in this subsection we indicate the distinctions between the plain and Janus cases.

An essential requirement for particles to deposit at the rim of an evaporating drop is that the drop be large enough: if the drop is too small it evaporates, or at least decays into a thin pancake, before the flow field is established and the particles are able to move to the rim. This behavior was first observed experimentally by Shen *et al.* [22], and we have reproduced it in simulations. The drop shown in Fig. 2 has a radius of about 15 nm, whereas in similar simulations for drops whose initial radius is around 5 nm, we see that the particles deposit roughly uniformly over the drops interior: see Fig. 8. Initially small evaporating droplets produce a somewhat uniform deposition pattern for plain particles, but some chain-like structure is evident in the Janus case. For larger droplets the deposit occurs preferentially at the rim, and in the Janus deposits chain formation is very evident.

A second requirement for deposition to occur at the drop rim is that the liquid must have adequate thermal contact with the solid to set up the flow field seen above [25]. We have investigated this issue by adjusting the interaction between the liquid and the wall: in Eq. 1 we varied the coefficient of the attractive r^{-6} term c_{fw} between 0 (pure short-distance repulsion – hydrophobic wall) and 1 (standard strength attraction – completely wetting wall) [20] and observed the resulting solid pattern. Independently, we measured the thermal conductance for each value of interaction strength by simulating a slab of liquid completely filling the gap between two atomic walls held at different temperatures. As the attractive strength decreased from 1 to 0, the amount of temperature slip (or, equivalently, Kapitza resistance) at the wall increased so that the thermal conductance decreased, approximately linearly, and ultimately by a factor of nearly 10 – see the left frame in Fig. 9). Correspondingly, as the wall attractive strength decreased the resulting pattern of solid particles varied from the rim deposit shown above to a random distribution, which is quite like that shown in the left panel of Fig. 8. More quantitatively, in the right frame of Fig. 9 we compare the (ensemble-averaged) radial distributions of the deposited particles for two different fluid-
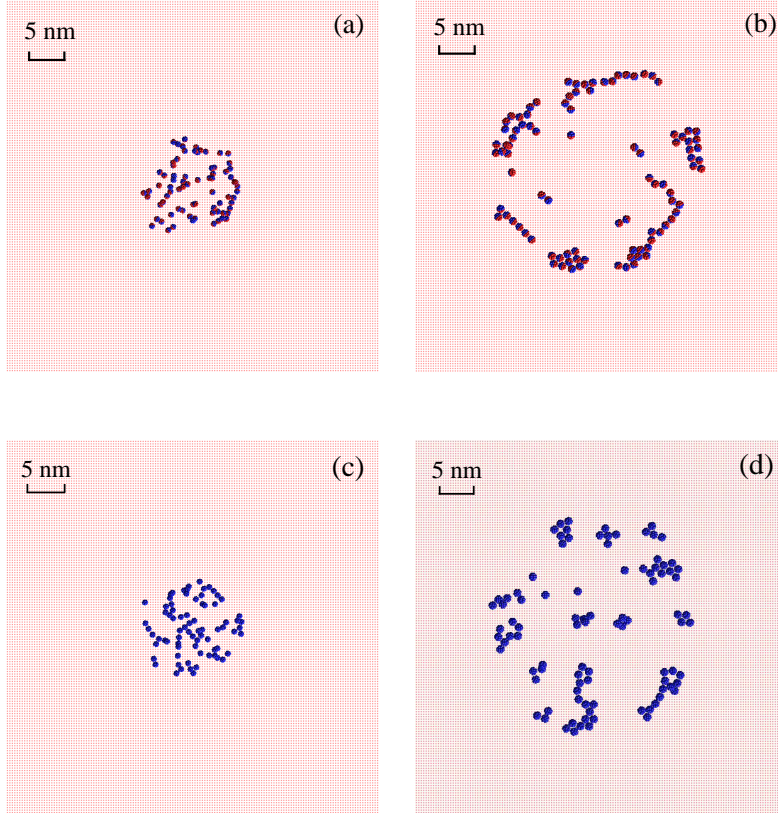
FIG. 8. (Color online) Top row: Janus particle deposit for evaporated drops of initial radius (a) 5 nm and (b) 15 nm. Bottom row: same for plain particles with initial radii (c) 5 nm and (d) 15 nm.

solid interaction strengths. Lowering the value of c_{fw} from 1.0 to 0.8 shifts the distribution from a sharp peak at the rim to a broader shape centered in the interior. In contrast, the strength of the fluid-particle interaction has very little effect on the structure of the deposit: varying its value from 0.5 to 1.0, for example, is observed to have almost no effect on the radial distribution. The effects of substrate thermal resistance and conductance on evaporation have been studied more systematically by Dunn *et al.* [26, 27].

The detailed structure of the deposit is an important consideration in potential applications to evaporative self-assembly. We saw above that particles with Janus surface properties would, under the right conditions, form a rim deposit with chain-like structures. This behavior is confirmed by experimental observations of gold-capped sulfated-polystyrene Janus particle-laden droplets during drying [28]. The chaining behavior is a result of the attractive interaction between the gold caps and the sulfated polystyrene half of the Janus particles.
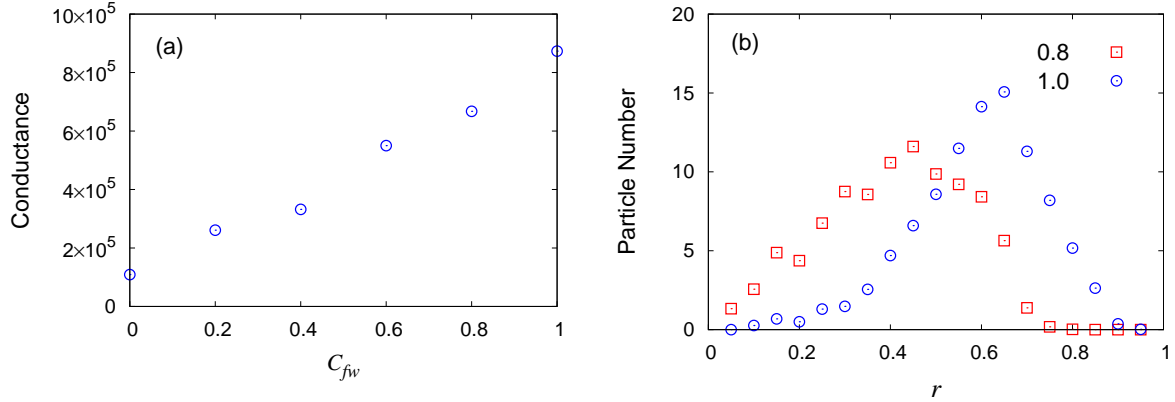
FIG. 9. (Color online) (a) Thermal conductance vs. attractive wall-liquid interaction strength c_{fw} in the Lennard-Jones potential. (b) Ensemble averaged radial distribution of deposited Janus particles for two different wall-liquid interaction strengths: red ($\square$) $c_{fw} = 0.8$ and blue ($\odot$) $c_{fw} = 1.0$.
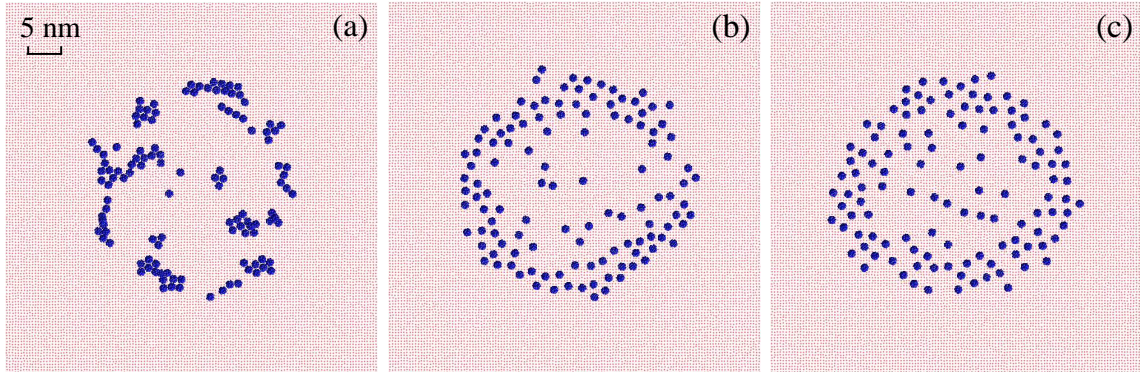

FIG. 10. Effects of adding a charge to a plain particle: deposition patterns for (a) charge 0, (b) charge 4 and (c) charge 8.

Additional experiments investigated the effect of particle surface charge on the deposition behavior [28, 29]. The presence of sulfate groups on the surface of the particles results in an overall negative surface charge, which can be screened by the addition of salt. Sulfated polystyrene particles in deionized water form hexagonal close-packed, highly ordered layers at the rim, whereas formation of randomly packed particle layers is observed in 10 mM aqueous NaCl solution. In contrast, Janus particles show random assembly at all electrolyte concentrations. These results motivated us to study the effect of charge on the deposit structure of uniform particles. In Fig. 10, we show the deposits that result when the charge

on a symmetric particle increases from 0 to 4 and then to 8. In the simulations, a charge of the appropriate magnitude is placed on randomly chosen individual atoms within each particle, and a Coulomb interaction is added to the Lennard-Jones potential. The neutral case resembles the random packing observed in the 10 mM case. The charge 8 situation models the case where the particles carry a charge, *i.e.*, deposition in deionized water. It is apparent from the right panel of Fig. 10 that the particles tend toward assembling at the rim and a regular packing [30], but that the drop volume is not sufficient to enable long enough evaporation times to achieve close packing at the rim.

III.   DISCUSSION AND CONCLUSION

We have shown that straightforward, medium-scale MD simulations can easily capture most of the salient features in the evaporation of particle-laden droplets. Aside from demonstrating that nano-scale and micron-scale systems behave in a similar way with regard to the behavior of the particles, we were able to measure continuum fields such as velocity within the droplet, along with the profile of the evaporative flux, which drives the process. Using standard methods, we have also measured the density, temperature and stress fields (but not reported here) within the droplet. In addition, we were able to show the existence of a minimum drop size for rim deposition, and verify the importance of adequate thermal coupling between liquid and solid. Furthermore, the simulations reveal the connection between particle interactions and deposit structure, and indicate some limitations in continuum modeling for nanodrops. The significance of these results is that simple simulations provide a viable method for both testing the theoretical underpinnings of the process and for predicting the nature of the outcome – the structure of the resulting particle deposit. Indeed, Cheng and Grest [31] have recently used similar MD simulations to examine the defect and grain boundary structure of the deposit formed by an evaporating particle-laden liquid film. In this paper we have focused on the most important aspect of the continuum flow, the velocity field and the evaporative flux, but any other quantity which can be determined from atomic variables is equally accessible.

ACKNOWLEDGMENTS

---

[1] S. Jiang, Q. Chen, M. Tripathy, E. Luitjen, K. S. Schweitzer and S. Granick, Adv. Mater. **22**, 1060 (2010).

[2] R. D. Deegan, O. Bakajin, T. F. Dupont, G. Huber, S. R. Nagel and T. A. Witten, Nature **389**, 827 (1997).

[3] R. D. Deegan, Phys. Rev. E **61**, 475 (2000).

[4] T. P. Bigioni, X.-M. Lin, T. T. Nguyen, E. I. Corwin, T. A. Witten and H. M. Jaeger, Nature Mater. **5**, 265 (2006).

[5] H. Bodihuel and J. Lang, Soft Matter **6**, 5451 (2010).

[6] R. Bhardwaj, X. Feng, P. Somasundaran and D. Asttinger. Langmuir, **26**, 7833 (2010).

[7] K. L. Maki and S. Kumar, Langmuir, **27**, 11347 (2011).

[8] N. Murisic and L. Kondic, J. Fluid Mech **679**, 219 (2011)

[9] R. D. Deegan, O. Bakajin, T. F. Dupont, G. Huber, S. R. Nagel and T. A. Witten, Phys. Rev. E **62**, 756 (2000).

[10] Y. O. Popov, Phys. Rev. **71**, 036313 (2005).

[11] H. Hu and R. G. Larson, J. Phys. Chem. B **106**, 1334 (2002).

[12] H. Hu and R. G. Larson, Langmuir **21**, 3963 (2005).

[13] T. Okuzono, M. Kobayashi and M. Doi, Phys. Rev. E **80**, 021603 (2009).

[14] A. Cazabat and G. Guéna, Soft Matter **6**, 2591 (2010).

[15] F. Guzman and I. Kretzschmar, Unpublished, City College of New York (2010).

[16] M. P. Allen and D. J. Tildesley, *Computer Simulation of Liquids* (Oxford, New York, 1987)

[17] D. Frenkel and B. Smit, *Understanding Molecular Simulation*, 2nd ed. (Academic, New York, 2002).

[18] D. C. Rapaport. *The Art of Molecular Dynamics Simulation*, 2nd ed. (Cambridge, New York, 1995)

[19] J. Pérez-Pellitero, P. Ungerer, C. Orkoulas and A. D. Mackie, J. Chem. Phys. **125**, 054515 (2006).

[20] J. Koplik, T. S. Lo, M. Rauscher and S. Dietrich, Phys. Fluids **18**, 031104 (2006).

[21] P.G. DeGennes, Rev. Mod. Phys. **57**, 827 (1985).

[22] X. Shen, C.-M. Ho and T.-S. Wong, J. Phys. Chem B **114**, 5269 (2010)

[23] J. J. Magda, M. Tirrell and H. T. Davis, J. Chem. Phys. **83** 1888 (1985)

[24] J. P. Burelbach, S. G. Bankoff and S. H. Davis, J. Fluid Mech. **195**, 463 (1988).

[25] B. H. Kim, A. Beskok and T. Cagiri, J. Chem. Phys. **129**, 174701 (2008).

[26] G. J. Dunn, S. K. Wilson, B. R. Duffy, S. David and K. Sefiane, J. Fluid Mech. **623**, 329 (2009).

[27] G. J. Dunn, S. K. Wilson, B. R. Duffy, and K. Sefiane, Phys. Fluids **21**, 052101 (2009).

[28] F. Guzman, E. Cranston, M. Rutlend and I. Kretzschmar, to be published (2012).

[29] S. C. Rödner, P. Wedin and L. Bergstrom, Langmuir **18**, 9327 (2002).

[30] Y. K. Koh and C. C. Wong, Langmuir **22**, 897 (2006).

[31] S. Cheng and G. S. Grest, J. Chem. Phys. **138**, 064701 (2013).